In-plane anisotropy of the electric field gradient in $Ba(Fe_{1-x}Co_x)_2As_2$ observed by ^{75}As NMR

Masayuki Toyoda, Akihiro Ichikawa, Yoshiaki Kobayashi, Masatoshi Sato, and Masayuki Itoh
Department of Physics, Graduate School of Science, Nagoya University, Furo-cho, Chikusa-ku, Nagoya 464-8602, Japan

(Received 30 November 2017; revised manuscript received 18 March 2018; published 7 May 2018)

We have performed ^{75}As NMR measurements on single crystals to investigate the nematic behavior via the in-plane anisotropy of the electronic state at the As site far from Co impurities in the representative iron arsenides $Ba(Fe_{1-x}Co_x)_2As_2$. From the analysis of the angular dependence of the NMR satellites in the c plane using the binominal distribution, we find that there is the in-plane fourfold symmetry breaking, namely, the orthorhombic-type anisotropy in the electric field gradient (EFG) at the As site with no Co atom at the nearest neighboring Fe sites even in the tetragonal phase of both $BaFe_2As_2$ and $Ba(Fe_{1-x}Co_x)_2As_2 (x \neq 0)$. The NMR spectrum in the antiferromagnetically ordered state of $BaFe_2As_2$ is shown not to support a nanotwin model on the basis of the nematic order proposed from the pair-distribution analysis of neutron scattering data. Based on results of the x and temperature T dependences of the in-plane anisotropy in the wide x and T ranges, the symmetry breaking is concluded to come from the local orthorhombic domains induced by disorder such as Co impurities or lattice imperfections. Furthermore, we find that the asymmetry parameter of EFG η obeys the Curie-Weiss law which may be governed by nematic susceptibility, and the Weiss temperature becomes zero at $x_c \sim 0.05$ in $Ba(Fe_{1-x}Co_x)_2As_2$.

DOI: 10.1103/PhysRevB.97.174507

I. INTRODUCTION

In iron-based superconductors with multiorbitals, the orbital fluctuation (fluctuation in electron occupation on orbitals) is one of the important parameters which govern characteristic properties emerging together with structural, magnetic, and superconducting (SC) transitions. One of such properties related to orbital degrees of freedom is the nematic order and fluctuation. The local structure and local electronic state appear with a lower symmetry than the crystal structure in the tetragonal phase of the iron-based superconductors [1–4].

In general the iron-based superconductors have SC, antiferromagnetic (AFM), and nematic ordered phases. The transition from the paramagnetic phase to the nematic ordered phase is accompanied with the structural transition from the high-temperature (high-T) tetragonal to low-T orthorhombic phases [5–8]. Figure 1 shows the T versus Co concentration x phase diagram in representative iron-based superconductors, $Ba(Fe_{1-x}Co_x)_2As_2$ [8,9]. In this phase diagram, the nematic transition is accompanied with the structural transition at T_s, whereas a stripe-type AFM transition takes place at T_N equal to or lower than T_s. Also the nematic ordered phase is characterized by the breaking of the in-plane fourfold rotational (C_4) symmetry in electrical resistivity [1,10], magnetization [11], and crystal structure [12]. In several studies, the symmetry breaking is reported even in the tetragonal phase of $T_s < T < T^*$ where T^* is the temperature around which the nematic phase becomes appreciable with decreasing T [1,11,13]. The AFM and nematic phases are in proximity to the SC phase [8,9]. These characteristics make the orbital fluctuation mechanism of SC realistic, because the breaking of the in-plane C_4 symmetry in the tetragonal phase may be somewhat related to the short-range orbital ordering as the manifestation of the locally frozen or pinned orbital fluctuation [14–16]. On the other hand, the spin-nematic order and fluctuation due to the spin-lattice coupling have also been discussed [17–20].

Nuclear magnetic resonance (NMR) is a useful probe for studying magnetic and electronic properties of the Fe-based superconductors. Indeed, many NMR studies have been made to study local susceptibility, spin fluctuations, and SC properties of $Ba(Fe_{1-x}Co_x)_2As_2$ [21–32]. There are also NMR reports on the nematic phenomena in their tetragonal phases [33–39]. The in-plane anisotropy was reported to appear in the tetragonal phase of $Ba(Fe_{1-x}Co_x)_2As_2$ [33,34] and $BaFe_2(As_{1-x}P_x)_2$ [35]. In $BaFe_2(As_{1-x}P_x)_2$ the orbital ordering of Fe $3d_{xz}$ and $3d_{yz}$ electrons was pointed out via the electric field gradient (EFG) measurement [35]. Local nematic susceptibility was studied from the electric quadrupole splitting under a strain field in $BaFe_2As_2$ [36]. From measurements of the nuclear spin-lattice relaxation rate, glassy nematic fluctuations were discussed in $Ba(Fe_{1-x}Co_x)_2As_2$ [37,38] and $BaFe_2(As_{1-x}P_x)_2$ [39]. Thus NMR is useful to study the nematic phenomena. However, the EFG measurement on $Ba(Fe_{1-x}Co_x)_2As_2$ with a wide range of Co concentration has been insufficiently made. A detailed EFG study is desired to understand the nematic phenomena in the wide-range carrier number from a microscopic point of view.

In this paper we have performed ^{75}As NMR measurements on single crystals to investigate the in-plane anisotropy of the electronic state in the wide Co range of $Ba(Fe_{1-x}Co_x)_2As_2$. We present the results of the in-plane anisotropy in EFG at the ^{75}As nuclear position in the wide T and x ranges. The results show that the orbital order locally exists in the tetragonal phase which includes the $x \sim 0.08$ superconducting sample without structural and magnetic transitions. We discuss the relation between the nematic behavior and lattice imperfection due to the doped Co impurity and/or defects. In particular, we present

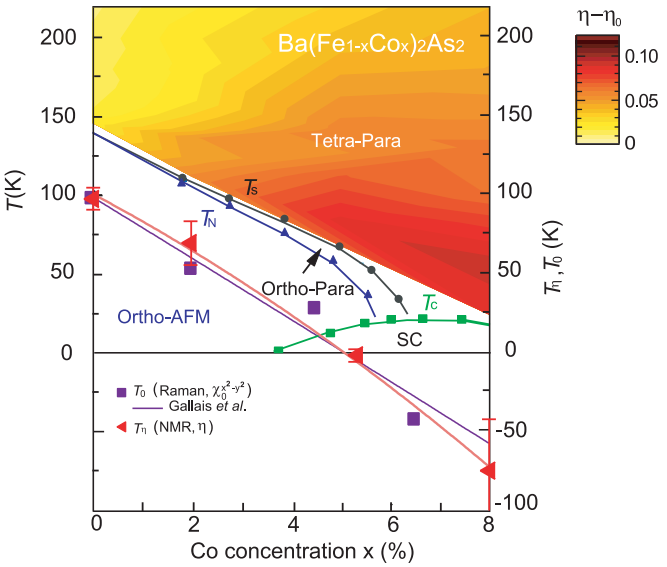

FIG. 1. Temperature T versus Co concentration x phase diagram of $Ba(Fe_{1-x}Co_x)_2As_2$ [9], where tetragonal-paramagnetic (Tetra-Para), orthorhombic-paramagnetic (Ortho-Para), orthorhombic-antiferromagnetic (Ortho-AFM), and superconducting (SC) phases appear. The Tetra-Ortho structural, AFM, and SC transition temperatures are denoted by T_s, T_N, and T_c, respectively. The contour plot of the asymmetry parameter of the electric field gradient at the As site $\eta - \eta_0$, where η obeys the Curie-Weiss law $\eta = C_\eta/(T - T_\eta) + \eta_0$ with the Weiss temperature T_η and constants C_η and η_0, is also displayed in the Tetra-Para phase (see text). The x dependence of T_η is presented with that of the Weiss temperature of Raman nematic susceptibility $\chi_0^{x^2-y^2}$, T_0 [40,41].

the Curie-Weiss behavior observed in the T dependence of the asymmetry parameter of EFG η where the Weiss temperature becomes zero at $x_c \sim 0.05$.

II. EXPERIMENTAL PROCEDURE

Single crystals of $Ba(Fe_{1-x}Co_x)_2As_2$ utilized in the present NMR measurement were grown by the self-flux method [42]. The Co concentration was estimated from comparing the c-axis length measured by the x-ray diffraction with its x dependence reported in Ref. [42]. The $x = 0$ sample, which was annealed in vacuum at 800 °C for 24 hours, exhibited the structural transition at $T_s = 143$ K [12] slightly lower than the reported temperatures [9,12]. The as-grown $x = 0.02$ and 0.05 samples were confirmed to have $T_s \sim 100$ and 60 K, respectively, whereas the $x = 0.08$ sample exhibited no structural and AFM transitions, and only a SC transition at $T_c = 23$ K [34].

^{75}As NMR measurements were made on the $Ba(Fe_{1-x}Co_x)_2As_2$ single crystals using a conventional phase-coherent pulsed NMR equipment with a superconducting magnet of a magnetic field $H_0 = 7.6966$, 7.6999, or 7.7023 T. A two-axis goniometer was utilized to rotate the single crystals in the magnetic field. The Fourier-transformed (FT) NMR spectrum was obtained by superposing FT spectra measured for a spin-echo signal step-by-step as a function of the NMR frequency. An ^{75}As nucleus has the nuclear spin $I = 3/2$ and the gyromagnetic ratio $\gamma = 2\pi \times 7.2919$ MHz/T. Each single crystal with typical size of $2.0 \times 2.0 \times 0.1$ mm^3 was inserted into an NMR coil where no glue pasting it to the sample holder was utilized to avoid the orthorhombic distortion due to the external stress. This stress is confirmed to come from the difference in the thermal dilatation coefficient between the sample and the glue [43,44].

III. EXPERIMENTAL RESULTS AND DISCUSSION

A. NMR spectrum

1. $BaFe_2As_2$

Figure 2(a) shows the ^{75}As NMR spectra at 135 K in the orthorhombic AFM phase and at 150 K in the tetragonal paramagnetic phase with H_0 parallel to the Fe-As direction within the c plane in the $BaFe_2As_2$ single crystal. In this paper the direction of the Fe-As bond projected on the c plane (the tetragonal a_T axis or [110] direction of the orthorhombic unit cell) is described as the Fe-As direction. The NMR spectrum has center and two satellite lines split by the electric quadrupole interaction in the tetragonal paramagnetic phase, whereas it moves to a high frequency in the orthorhombic AFM phase. Furthermore, each satellite line is split into two spectra, A and B, with tilting H_0 from the Fe-As direction (the azimuthal angle $\phi = 45°$) in the c plane as seen in Fig. 2(b) which shows the ϕ dependence of the NMR spectrum in the c plane at 135 K. Here ϕ is the angle of H_0 measured from the Fe-Fe direction in the c plane.

In general, the resonance frequency of the $m \leftrightarrow m-1$ ($m = I, I-1, \ldots, -I+1$) transition in an effective field $H_{\rm eff}$ is expressed in the first-order perturbation of the electric quadrupole interaction as [23,45]

$$\nu_{m\leftrightarrow m-1} = \frac{\gamma}{2\pi}H_{\rm eff} + \frac{1}{2}\nu_Q\left(m - \frac{1}{2}\right)(3\cos^2\theta - 1 + \eta\sin^2\theta\cos 2\phi), \quad (1)$$

where the angles θ and ϕ are the polar and azimuthal angles of $H_{\rm eff}$, respectively, in the xyz principal coordinate system of the EFG tensor. Also ν_Q ($= |\nu_z| = |\nu_x + \nu_y|$) is the nuclear electric quadrupole frequency where $\nu_\alpha = 3eV_{\alpha\alpha}Q/[2I(2I-1)h]$ ($\alpha = x, y, z$) with a principal component of the EFG tensor $V_{\alpha\alpha}$ ($|V_{xx}| \leqslant |V_{yy}| \leqslant |V_{zz}|$), the elementary charge e, the nuclear quadrupole moment Q, and the Plank's constant h. Also η is the asymmetry parameter of EFG defined as $\eta = |\nu_x - \nu_y|/|\nu_z|$.

In the AFM phase, the orthorhombic structure (space group $Fmmm$) requires that the a, b, and c axes are the principal axes of the EFG tensor. In Eq. (1), $H_{\rm eff}$ is expressed as $H_{\rm eff} = \sqrt{H_0^2 + H_{\rm in}^2}$ with the internal field $H_{\rm in}$ parallel to the c axis, mainly the transferred hyperfine (TH) field coming from the nearest-neighbor (nn) Fe magnetic moments which form the stripe-type AFM order along the a axis [23]. The ϕ dependence of the nuclear electric quadrupole splitting $\delta\nu = (\nu_{3/2\leftrightarrow 1/2} - \nu_{-1/2\leftrightarrow -3/2})/2$ with H_0 rotated in the c plane at 135 K is shown in the inset of Fig. 2(b). Here $\delta\nu$ is expressed as

$$\delta\nu = \tfrac{1}{2}\nu_Q(3\cos^2\theta - 1 + \eta\sin^2\theta\cos 2\phi). \quad (2)$$

The experimental ϕ dependence of $|\delta\nu|$ is well reproduced by Eq. (2) with $H_{\rm in} = 0.82$ T, $\nu_Q = 2.203$ MHz, $\eta = 0.824$, and

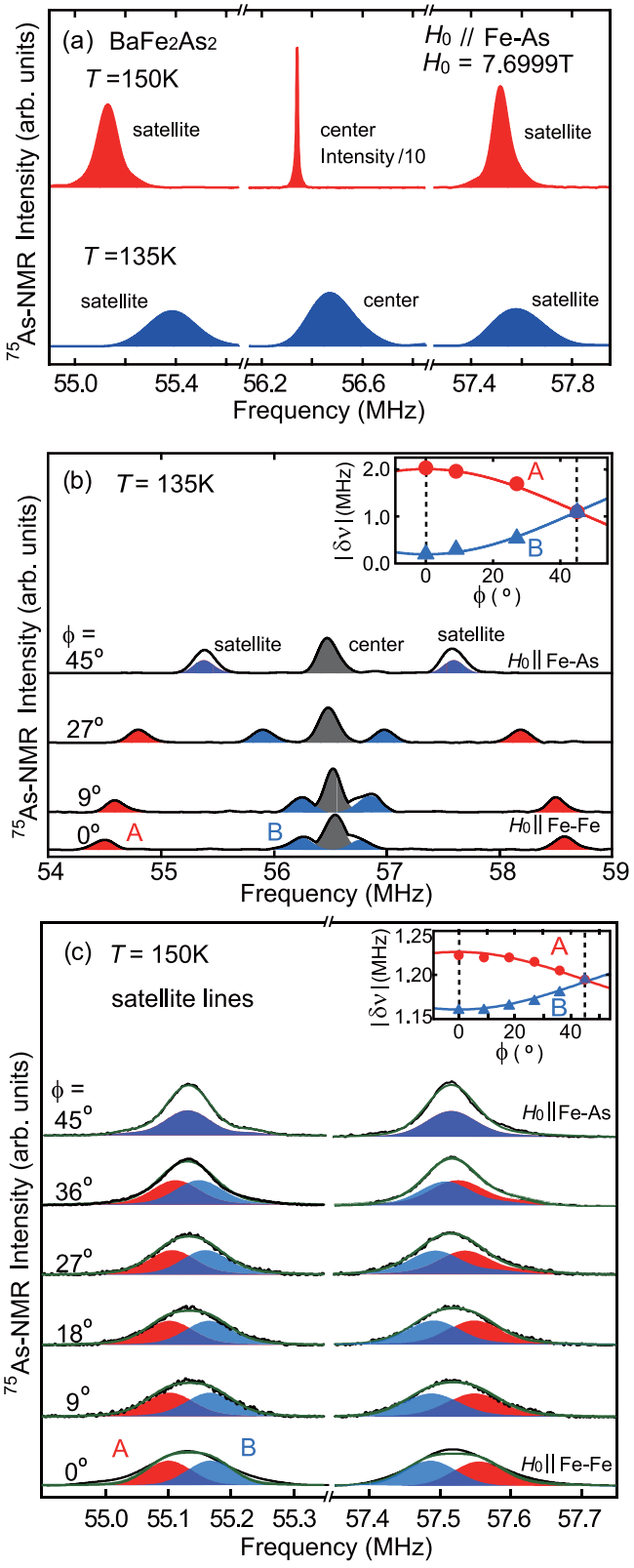

FIG. 2. (a) ^{75}As NMR spectra with H_0 (=7.6999 T) parallel to the Fe-Fe direction at 135 and 150 K in the $BaFe_2As_2$ single crystal. Angle ϕ dependence of the NMR spectrum at (b) 135 and (c) 150 K with H_0 rotated in the c plane. Each satellite line is composed of two Gaussian-like spectra A (red) and B (blue). The insets show the angle ϕ dependence of the nuclear electric quadrupole splitting $|\delta\nu|$ in the c plane.

$z \parallel c$ as presented by the solid curves in the inset. Note that the angles θ and ϕ of $H_{\rm eff}$ is governed by H_0 due to the small value of $H_{\rm in}/H_0 = 0.11$. Thus the presence of the A and B spectra is ascribed to the orthorhombic twin structure. These results agree with the previous report [23].

On the other hand, in the tetragonal paramagnetic phase (space group $I4/mmm$), the tetragonal symmetry requires that $\eta = 0$ corresponding to no ϕ dependence of $\delta\nu$ in the tetragonal c plane, x and y are located in the c plane, and $z \parallel c$. However, the lower and upper satellite lines show the ϕ dependence with H rotated in the c plane at 150 K as shown in Fig. 2(c). Each satellite spectrum is fitted by the summation of two spectra A and B which are assumed to have the Gaussian-like shape observed for H_0 parallel to the Fe-As direction, because the A and B spectra become one spectrum for $H_0 \parallel$ Fe-As as seen in Fig. 2(c). In this fitting, the central NMR frequency is a fitting parameter with keeping the same intensity and the same spectrum width of the Fe-As direction for the two spectra. The inset of Fig. 2(c) shows the ϕ dependence of $|\delta\nu|$ for the A and B spectra. In a paramagnetic phase, the angles θ and ϕ in Eq. (2) are the polar and azimuthal angles of H_0, respectively, in the xyz principal coordinate system of the EFG tensor. The ϕ dependence of $|\delta\nu|$ is well reproduced by Eq. (2) with $\nu_Q = 2.39$ MHz and $\eta = 0.025$ as seen in the inset of Fig. 2(c). The ν_Q value is consistent with the reported result [23,35]. The nonzero η value in the c plane clearly shows that the C_4 symmetry is locally broken in the tetragonal phase of $BaFe_2As_2$. Also the two spectra, A and B, come from two local orthorhombic regions with the local symmetry axes, a and b, perpendicular to each other in the microscopic scale. However, they form the tetragonal crystal structure with the symmetry axes, $a_{\rm T}$ and $b_{\rm T}$, parallel to the Fe-As directions in the macroscopic scale.

Recently, Niedziera *et al.* carried out the pair distribution function (PDF) analysis for the neutron scattering data in the orthorhombic AFM phase of $BaFe_2As_2$ [46]. They point out that the nematic order results in the local atomic structure significantly different from that of the average structure in the c plane. Based on this local structure, they propose a nanotwin model which locally affects the alignment of the AFM moments different from the stripe-type order in the AFM phase. An As site has $H_{\rm in}$ via the TH interaction between the As nucleus and its four nn Fe magnetic moments. In this model, there are locally some arrangements of the Fe magnetic moments parallel or antiparallel to the a axis such as the AFM1-type (stripe-type) arrangement and the AFM2-type arrangement where one Fe moment in the AFM1-type arrangement is inversed as shown in the inset of Fig. 3. Among the arrangements, the AFM1-type arrangement provides $H_{\rm in}$ parallel to the c axis, whereas the AFM2-type one leads to a component of $H_{\rm in}$ in the c plane. For the AFM2-type arrangement, we can calculate the NMR frequency $\nu_{\rm res}$ from the resonance condition $\nu_{\rm res} = \frac{\gamma}{2\pi}|\mathbf{H}_0 + \mathbf{H}_{\rm in}|$ where $\mathbf{H}_{\rm in} = \sum_{j=1}^{4} \mathbf{A}_j^{\rm hf}\mathbf{M}_j = 2M(A_{aa}^{\rm hf}, A_{ab}^{\rm hf}, A_{ac}^{\rm hf})$ with the components of the TH coupling tensor, $A_{aa}^{\rm hf} = 0.66\ {\rm T}/\mu_{\rm B}$ and $A_{ac}^{\rm hf} = 0.43\ {\rm T}/\mu_{\rm B}$ [23], and the Fe magnetic moment of $M = 1.04\ \mu_{\rm B}$ parallel to the a axis (Fe-Fe direction) [46]. Here we assume as $A_{ab}^{\rm hf} = 0$ and $0.43\ {\rm T}/\mu_{\rm B}$, because there is no available value of $A_{ab}^{\rm hf}$. Thus the AFM2 spectrum has to appear around $\nu_{\rm res} = 64$ or 68 MHz in addition to the AFM1 spectrum observed at ~57 MHz as shown in Fig. 3 which presents the

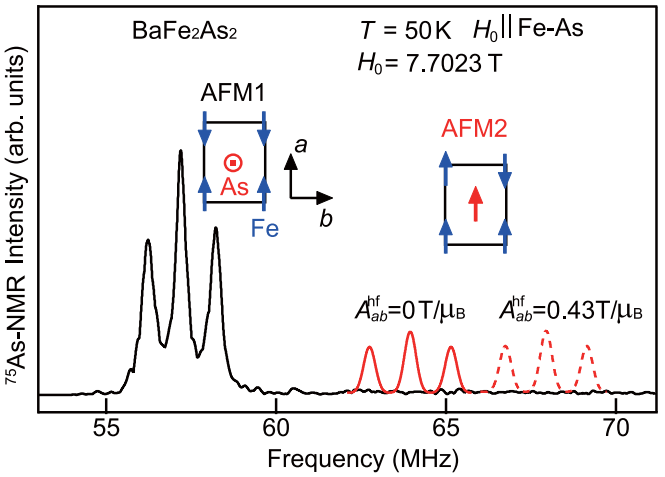

FIG. 3. ^{75}As NMR spectrum at 50 K with H_0 (=7.7023 T) parallel to the Fe-As direction in $BaFe_2As_2$. The inset shows the local AFM1-type (stripe-type) and the AFM2-type arrangements for the nearest-neighbor four Fe moments (blue arrows) of the As site with the internal field denoted by the red arrows. The red solid and dashed spectra are calculated spectra with the electric quadrupole splitting for the local AFM2-type arrangement within a model of the magnetic structure [46] in the antiferromagnetic phase (see text).

^{75}As NMR spectrum at 50 K with H_0 (=7.7023 T) parallel to the Fe-As direction in the c plane. The calculated spectra with the electric quadrupole splitting are convoluted by a Gaussian with full width at half maximum (FWHM) of 0.3 MHz and the ratio of AFM2 to AFM1 is assumed to be 1:4 as discussed in Ref. [46]. Observation of no AFM2 NMR spectrum indicates that the present NMR result does not support the proposed model.

2. $Ba(Fe_{1-x}Co_x)_2As_2$

Figure 4 shows ^{75}As NMR spectra at 150 K with H_0 parallel to the Fe-As direction in the tetragonal phase of $Ba(Fe_{1-x}Co_x)_2As_2$ with $x = 0.02, 0.08$, and, for comparison, $x = 0$. The Co doping induces the increase in spectrum width

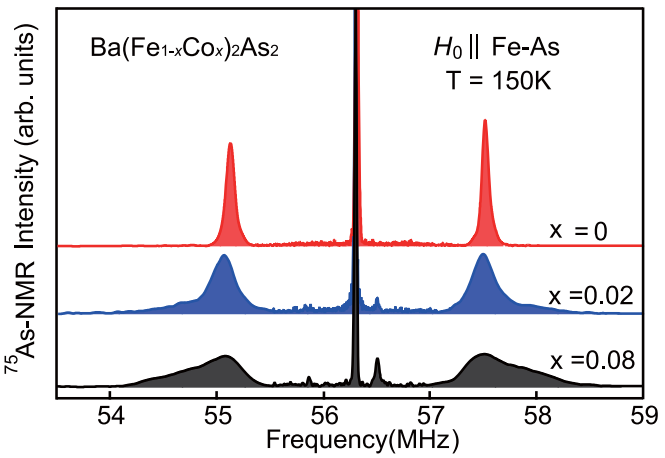

FIG. 4. ^{75}As NMR spectra with $H_0 = 7.6999$ ($x = 0$ and 0.08) or 7.6964 T ($x = 0.02$) parallel to the Fe-As direction at 150 K in the $Ba(Fe_{1-x}Co_x)_2As_2$ single crystals.

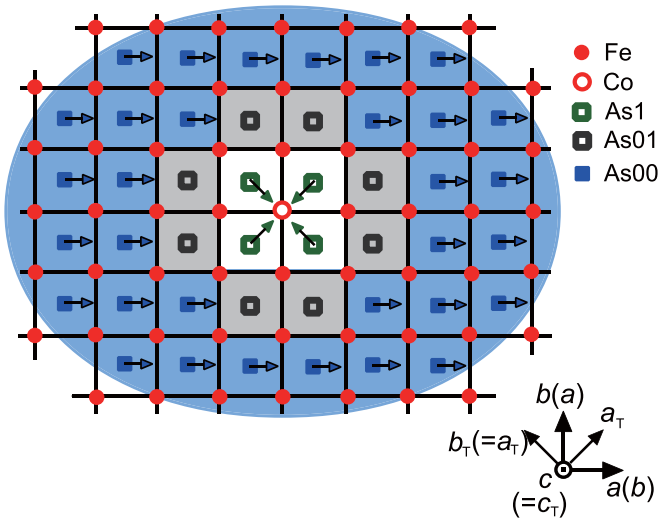

FIG. 5. Schematic local configuration of the As00, As01, and As1 sites around a Co atom projected on the c plane in $Ba(Fe_{1-x}Co_x)_2As_2$. The symbols As00, As01, and As1 represent the As sites with no Co atom at the nearest-neighbor (nn) and next-nearest-neighbor (nnn) Fe sites, no Co at the nn Fe sites and one Co at the nnn Fe sites, and one Co at the nn Fe sites, respectively. The blue arrows represent the direction of the x or y principal axis of the EGF tensor at the As00 site, whereas the green ones denote the direction of the z axis at the As1 site. The a, b, and c axes are the orthorhombic axes in the microscopic scale, whereas a_T, b_T, and c_T are the tetragonal axes in the macroscopic scale.

of both the center and satellite spectra. In addition to the main center line, two weak center lines appear at ~55.9 and ~56.5 MHz. The main center line stems from the As site with no Co at the four nn Fe sites, As0, as seen in Fig. 5 which schematically shows the As sites around a Co atom, whereas the additional lines come from the As site with one Co, As1, as reported by Ning *et al.* [27]. The spectrum intensity ratio of As0 to As1 is reproduced by the binominal distribution ${}_4C_n x^n (1-x)^{4-n}$ for $n = 0$ and 1 where n is the number of the Co atom occupying the nn four Fe sites.

We present the upper satellite lines coming from the As0 site of the $x = 0.02$ sample at 110 K and the $x = 0.08$ sample at 50 K with H_0 parallel to the Fe-Fe and Fe-As directions in Fig. 6. Each satellite is decomposed into several spectra, because the As0 site is split into the As0n sites with n (= 0–8) Co atoms at the eight next-nearest-neighbor (nnn) Fe sites as displayed in Fig. 5. By assuming that the number of the As0n sites may obey the binominal distribution of ${}_8C_n x^n (1-x)^{8-n}$, the ratio of As00:As01:As02:As0n ($n \geqslant 3$) is evaluated as 85:14:1:0 for $x = 0.02$ and 51:36:11:2 for $x = 0.08$ [33,34]. Furthermore, we assume that the As00 spectrum may be split into two spectra as observed in the $x = 0$ sample. Also the others As0n ($n \geqslant 1$) are assumed not to be split, because several configurations around a Co impurity lead to the inhomogeneous spectrum broadening behind which a spectrum due to each configuration is hidden. By fitting the spectra to the summation of Gaussians, the satellite spectrum of $x = 0.02$ can be traced by the two As00, A (red) and B (blue), and one As01 (gray) Gaussians as seen in Figs. 6(a) and 6(b), whereas the spectrum of $x = 0.08$ is composed

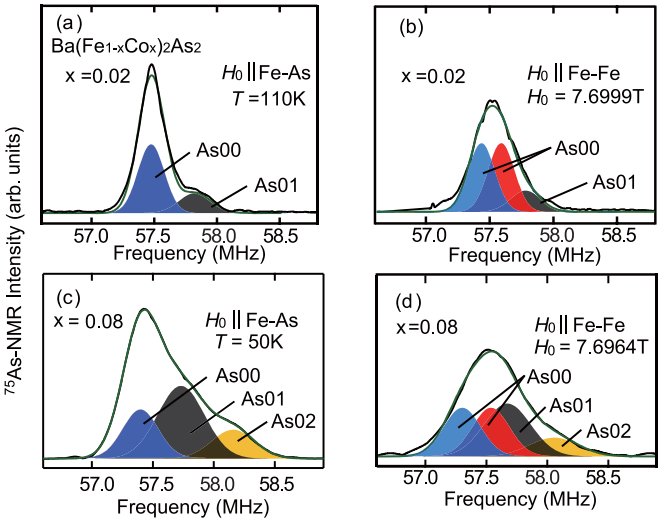

FIG. 6. ^{75}As NMR upper satellite lines coming from the As0 site, which has no Co atom at the four nearest-neighbor Fe sites, with H_0 parallel to the Fe-As and Fe-Fe directions for (a), (b) $x = 0.02$ at 110 K, and (c), (d) $x = 0.08$ at 50 K in the $Ba(Fe_{1-x}Co_x)_2As_2$ single crystals. Each line is composed of spectra from the As00 (red and blue), As01 (gray), and As02 (yellow) sites with no, one, and two Co atoms, respectively, at the eight next-nearest-neighbor Fe sites among the As0 sites. Note that the red and blue spectra are overlapped in the As00 spectra with H_0 parallel to the Fe-As direction in (a) and (c).

of two As00, A (red) and B (blue), one As01 (gray), and one As02 (yellow) Gaussians as seen in Figs. 6(c) and 6(d). Here note that the two As00 spectra A (red) and B (blue) are overlapped for H_0 parallel to the Fe-As direction. Thus the As00 spectrum is traced by the two Gaussians in each spectrum of the $x = 0.02$ and 0.08 samples. This shows that there are locally two orthorhombic regions in the Co-doped system $Ba(Fe_{1-x}Co_x)_2As_2$ as well as in $BaFe_2As_2$. The presence of the two regions is reported for $BaFe_2(As_{1-x}P_x)_2$ [35].

Figure 7(a) shows the ϕ dependence of the ^{75}As lower and upper satellite lines at 110 K with H_0 rotated within the c plane in the tetragonal phase for the $x = 0.02$ sample. The ϕ dependence of $|\delta\nu|$ is shown for each As00 satellite line in the inset of Fig. 7(a). From the analysis of the $|\delta\nu|$ data based on Eq. (2), we obtain $\nu_Q = 2.31$ MHz and $\eta = 0.071$ for $x = 0.02$. On the other hand, $|\delta\nu|$ of the As01 satellite spectrum empirically obeys the relation, $|\delta\nu| = \delta\nu_0 - \delta\nu_1 \cos 4\phi$ with constants $\delta\nu_0 = 1.466$ MHz and $\delta\nu_1 = 0.030$ MHz, as seen in the inset of Fig. 7(a). This As01 spectrum comes from As nuclei at the eight As01 sites around a Co atom in one orthorhombic domain (see Fig. 5). Since an As nucleus at each As01 site has a different NMR frequency governed by its local symmetry and dependent on the direction of H_0, the As01 spectrum is the superposition of the eight spectra. In the single-impurity model, if the z axis of the EFG tensor is parallel to the c axis, $\delta\nu$ for the center of gravity in the As01 spectrum is expressed as

$$\delta\nu = \frac{\nu_Q}{16} \sum_{j=1}^{8} \{-1 + \eta \cos(2\phi - \phi_{0,j})\}, \qquad (3)$$

where $\phi_{0,j} (j = 1\text{–}8)$ is the angle between the a or b axis and the direction from the Co atom to the jth As01 position

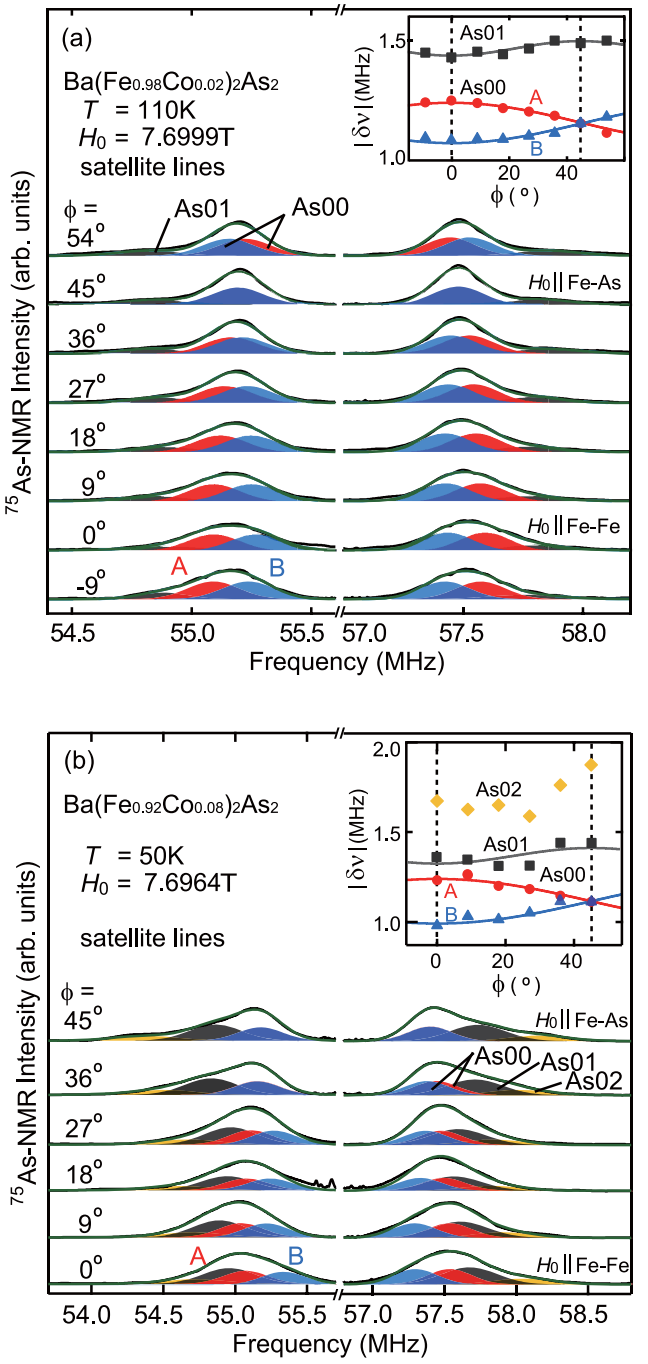

FIG. 7. Angle ϕ dependence of the ^{75}As lower and upper satellites with H_0 rotated in the c plane for (a) the $Ba(Fe_{0.98}Co_{0.02})_2As_2$ single crystal at 150 K and (b) the $Ba(Fe_{0.92}Co_{0.08})_2As_2$ single crystal at 50 K. The As0 spectrum coming from the Co site with no Co atom at the four nearest-neighbor (nn) Fe sites is decomposed into two Gaussians denoted by the red (A) and blue (B) curves. On the other hand, the As01 (As02) spectrum comes from the As01 (As02) site with no Co at the four nn and one (two) Co at the eight next-nearest-neighbor Fe sites. The insets show the angle ϕ dependence of the nuclear electric quadrupole splitting $|\delta\nu|$ for the As00, As01, and As02 spectra. The red and blue curves are the results of fitting the experimental data of the As00 spectra to Eq. (2). The gray curves are the results of fitting the data of the As01 spectrum to the phenomenological relation $|\delta\nu| = \delta\nu_0 - \delta\nu_1 \cos 4\phi$ with constants $\delta\nu_0$ and $\delta\nu_1$.

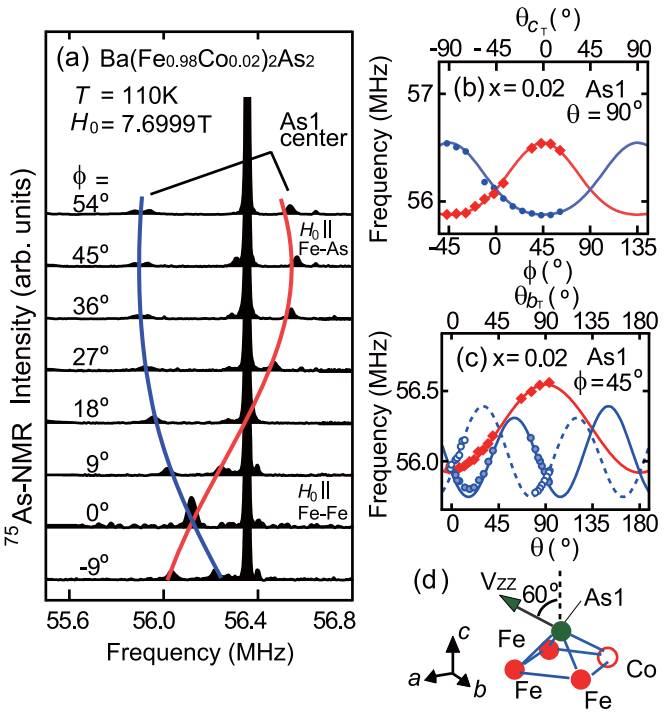

FIG. 8. (a) Angle ϕ dependence of the ^{75}As center lines with H_0 rotated in the c plane at 110 K in the $Ba(Fe_{0.98}Co_{0.02})_2As_2$ single crystal. The symbol As1 represents the center lines coming from the As1 sites with one Co atom at the four nearest-neighbor Fe sites. Angular dependences of the NMR frequency with H_0 rotated (b) in the c plane and (c) from the c axis to the Fe-As direction (in the b_T plane). The solid curves are results of fitting the data to Eq. (4). Also θ_{c_T} (θ_{b_T}) is the angle of H_0 measured from the a_T (c_T) axis in the c_T (b_T) plane. (d) Local square pyramid containing the As1 site. The arrow represents the direction of the z component of the electric field gradient tensor V_{zz}.

projected on the c plane. Furthermore, by taking account of two orthorhombic domains with the local a and b axes different from each other, we obtain $|\delta\nu| = \nu_Q$ due to the cancellation of the angular term in the superposition of the satellite spectra coming from As nuclei at the 16 As01 sites. This is consistent with the observed $|\delta\nu|$ having the dominant constant term $\delta\nu_0$. The weak angle dependence may be ascribed to deviation from the direction assumed for the z principal axis of the EFG tensor, unbalance between two orthorhombic domains, and so on.

For the $x = 0.08$ sample, we obtain $\nu_Q = 2.21$ MHz and $\eta = 0.114$ from the analysis of the ϕ dependence of $|\delta\nu|$ for the As00 spectrum in Fig. 7(b) which shows the ϕ dependence of the ^{75}As lower and upper satellite lines at 50 K with H_0 rotated within the c plane. The As01 spectrum roughly shows the weak angle dependence of $|\delta\nu|$ with $\delta\nu_0 = 1.354$ and $\delta\nu_1 = 0.016$ MHz as well as in the $x = 0.02$ sample as seen in the inset of Fig. 7(b). The complicated angle dependence is observed for the As02 spectrum, because many As02 sites having two Co atoms at the nn Fe sites contribute to the As02 spectrum.

Thus we can reasonably identify the satellite NMR spectrum and monitor the nematic behavior via the angle dependence of the As00 satellite spectrum. The present results clearly show that there is the breaking of the C_4 symmetry in the wide Co range at least up to $x = 0.08$ in the tetragonal phase of $Ba(Fe_{1-x}Co_x)_2As_2$.

The As1 site provides the two additional center lines at 110 K in Fig. 8(a) which shows the ϕ dependence of the center lines with $H_0(= 7.6999\,\mathrm{T})$ rotated within the c plane in the $x = 0.02$ single crystal. The ϕ dependence of the NMR frequency in the c plane is displayed in 8(b), whereas its θ dependence with H_0 rotated from the c axis to the Fe-As direction ($\phi = 45°$) is displayed in Fig. 8(c). The little splitting in the As1 center line may be due to the slight misalignment of H_0 and the average value of the splitting is plotted in Figs. 8(b) and 8(c). As seen in Fig. 5, the As1 site with one Co atom at the four nn Fe sites is expected to provide two NMR spectra with H_0 rotated in the c plane ($\theta = 90°$) and three ones with H_0 rotated from the c axis to the Fe-As direction ($\phi = 45°$). For $I = 3/2$, the resonance frequency of the center line with H_0 rotated in the c plane, $\nu_{1/2\leftrightarrow -1/2}$, is expressed in the second-order perturbation of the electric quadrupole effect [47] in addition to the Knight shift [48] as

$$\begin{aligned}\nu_{1/2\leftrightarrow -1/2} = \nu_0\big(1 + k_{1,c_T} + k_{2,c_T}\cos 2\theta_{c_T} + k_{3,c_T}\sin 2\theta_{c_T}\big) \\ + \frac{4\nu_Q^2}{\nu_0 V_{zz}^2}\big(n_{c_T} + p_{c_T}\cos 2\theta_{c_T} + r_{c_T}\sin 2\theta_{c_T} \\ + u_{c_T}\cos 4\theta_{c_T} + v_{c_T}\sin 4\theta_{c_T}\big),\end{aligned} \tag{4}$$

with

$$\begin{aligned}k_{1,c_T} &= \big(K_{a_Ta_T} + K_{b_Tb_T}\big)/2, \\ k_{2,c_T} &= \big(K_{a_Ta_T} - K_{b_Tb_T}\big)/2, \\ k_{3,c_T} &= K_{a_Tb_T}, \\ n_{c_T} &= \frac{1}{192}\left\{9V_{c_Tc_T}^2 - 14\left[\left(\frac{V_{a_Ta_T} - V_{b_Tb_T}}{2}\right)^2 + V_{a_Tb_T}^2\right]\right. \\ &\quad \left. - 8\big(V_{a_Tb_T}^2 + V_{b_Tc_T}^2\big)\right\}, \\ p_{c_T} &= \frac{1}{32}\big[V_{c_Tc_T}\big(V_{a_Ta_T} - V_{b_Tb_T}\big) + 4\big(V_{b_Tc_T}^2 - V_{a_Tc_T}^2\big)\big], \\ r_{c_T} &= \frac{1}{16}\big(-V_{c_Tc_T}V_{a_Tb_T} + 4V_{c_Ta_T}V_{b_Tc_T}\big), \\ u_{c_T} &= \frac{3}{32}\left[\frac{\big(V_{a_Ta_T} - V_{b_Tb_T}\big)^2}{4} - V_{a_Tb_T}^2\right], \\ v_{c_T} &= -\frac{3}{32}\big(V_{a_Ta_T} - V_{b_Tb_T}\big)V_{a_Tb_T},\end{aligned}$$

where $\nu_0 = \gamma H_0/2\pi$, and $K_{\alpha\beta}$ ($\alpha, \beta = a_T, b_T, c_T$) and $V_{\alpha\beta}$ are components of the Knight shift and EFG tensors, respectively, in the tetragonal $a_Tb_Tc_T$ coordinate system introduced to simply express Eq. (4) (see Fig. 5). Also $\theta_{c_T}(= \phi - 45°)$ is the angle between the tetragonal a_T axis and H_0. The equations for the other two rotations are obtained by cyclic permutation of a_T, b_T, and c_T. We can fit the experimental data to Eq. (4) without taking the anisotropy of the Knight shift in account and obtain the components of the Knight shift and EFG tensors in the $a_Tb_Tc_T$ coordinate system. After diagonalization of the tensors, we obtain the isotropic Knight shift $K_{iso} = 0.237\%$, $\nu_Q = 14.9$ MHz, and $\eta = 0.63$. The principal z axis with the angle 60°

tilted from the c axis is found to be approximately parallel to the direction of the Co-As bond as displayed in Figs. 5 and 8(d).

The ν_Q value of the As1 site is quite larger than those of $\nu_Q = 2$–3 MHz reported for the As0 spectra [23,27,33]. This may be caused by the difference in charge amount at the As1 site induced by the Co substitution. However, with Co^{2+} ($3d^7$) doping in the background of the Fe^{2+} ($3d^6$), additional electrons in the Fe (Co) layer are generally itinerant and contribute to the chemical potential [49]. Thus the enhancement of ν_Q at the As1 site mainly stems from the change in the local crystal structure rather than the local charge distribution. We can conclude that the observed broadening of the center and satellite As0 spectra is due to the effect of Co in the *nnn* and more distinct Fe sites around the As0 site, while the As1 center line is strongly affected by one Co in the *nn* site in $Ba(Fe_{1-x}Co_x)_2As_2$.

B. Electric field gradient

We concentrate our attention on the electric field gradient (EFG) of the As00 site in $Ba(Fe_{1-x}Co_x)_2As_2$. As mentioned above, the presence of η in the As00 satellite spectrum clearly shows that there are locally two types of regions which have the orthorhombic structure with the local symmetry axes perpendicular to each other even in the tetragonal phase. This means that the symmetry breaking from the C_4 symmetry to the C_2 symmetry locally takes place in the tetragonal phase. This symmetry breaking is observed by the magnetization measurement on a tiny crystal [11] and the electronic Raman response [40,41] in no external stress, and the elastic resistivity [1] and shear modulus C_{66} [43,44] measurements in external stress. The precise structural analyses for $BaFe_2As_2$ in the wide T range through T_s using neutron diffraction indicates that the orthorhombic distortion appears even in the tetragonal phase [12]. From theoretical point of view, Inoue *et al.* numerically showed that an impurity induces two types of fluctuating local orbital order along the orthogonal Fe-Fe directions in about $7a \times 15a$ lattice [15]. Although the orbital fluctuation generally has no contribution to η, an internal stress due to sample imperfection, sample edge, and so on may induce a static local orbital order even in no external stress as observed in $BaFe_2As_2$. This local orbital order is considered to be driven by the doped Co impurity in $Ba(Fe_{1-x}Co_x)_2As_2$ as discussed for $BaFe_2(As_{1-x}P_x)_2$ [35]. This is supported by the NMR study on the ^{75}As nuclear spin-lattice relaxation rate $1/T_1$ for $Ba(Fe_{1-x}M_x)_2As_2$ (M = Co and Cu), where the T and x dependences of the distribution in $1/T_1$ were discussed on the basis of a random strain field due to the disorder induced by atomic substitution [37,38]. More recently, nematic susceptibility is discussed from the electric quadrupole splitting which is observed to be induced by a strain field in $BaFe_2As_2$ [36].

Based on the T and x dependences of the EFG parameters, we discuss their characteristics. Figure 9(a) shows the T dependences of η and $|\nu_a - \nu_b|/|\nu_a + \nu_b|$ in $Ba(Fe_{1-x}Co_x)_2As_2$, whereas the T dependence of $|\nu_a + \nu_b|(= \nu_Q)$ is presented in Fig. 9(b). In $BaFe_2As_2$, η gradually increases with decreasing T in the tetragonal phase, obeying the Curie-Weiss (CW) law $\eta = C_\eta/(T - T_\eta) + \eta_0$ with the Weiss temperature T_η and the constants C_η and η_0 listed in Table I. Here the values of the CW

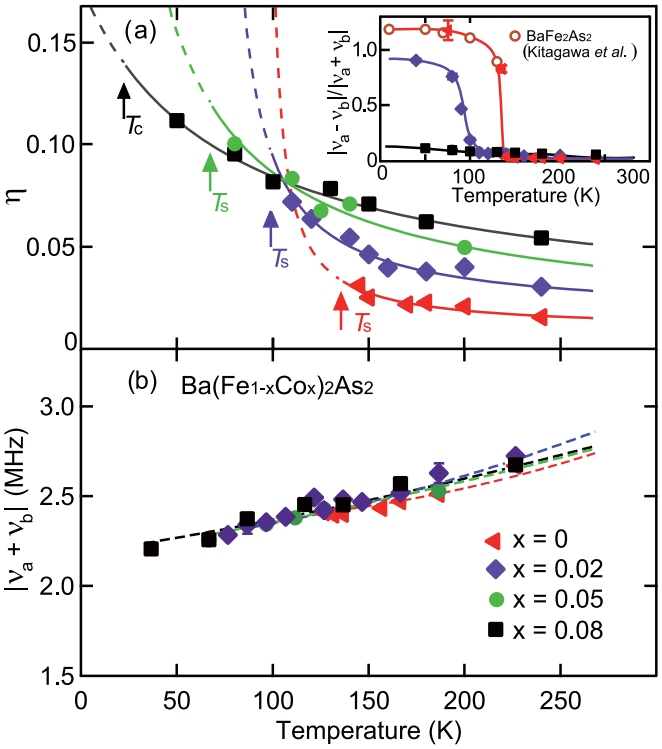

FIG. 9. Temperature dependences of (a) the asymmetry parameter of the electric field gradient η and (b) the nuclear electric quadrupole frequency $|\nu_a + \nu_b|(= \nu_Q)$ in $Ba(Fe_{1-x}Co_x)_2As_2$. The inset shows the temperature dependence of $|\nu_a - \nu_b|/|\nu_a + \nu_b|$ where the data of $BaFe_2As_2$ in Ref. [23] are included. The solid curves in (a) represent the results of fitting the experimental data to the Curie-Weiss law. The solid curves in the inset and the dashed curves are guide to the eye.

parameters are obtained from fitting the $1/\eta$ data to the relation $1/\eta = [C_\eta/(T - T_\eta) + \eta_0]^{-1}$. This result of η is consistent with the CW behavior of $d\eta/d\epsilon$ measured under a strain ϵ [36]. The CW term may come from the mixing of the As4p and Fe3d orbitals and be governed by nematic susceptibility, whereas η_0 may be ascribed to the charges outside the As ion in concern. The analysis and discussion on the CW behavior of the present η data of $Ba(Fe_{1-x}Co_x)_2As_2$ are presented with the η data of NaFeAs and LiFeAs to systematically understand the relation between η and nematic susceptibility of the Fe-based superconductors in our recent paper [50]. In particular, η is shown to scale with the Raman nematic susceptibility $\chi_0^{x^2-y^2}$ [40] in $BaFe_2As_2$. After $|\nu_a - \nu_b|/|\nu_a + \nu_b|$ rapidly

TABLE I. Weiss temperature T_η and constants, C_η and η_0, obtained by fitting the $1/\eta$ data, where η is the asymmetry parameter of the electric field gradient, to the relation $1/\eta = [C_\eta/(T - T_\eta) + \eta_0]^{-1}$ in the tetragonal phase of $Ba(Fe_{1-x}Co_x)_2As_2$.

x	C_η (K)	T_η (K)	η_0
0	0.98 ± 0.18	97 ± 8	0.0096 ± 0.0020
0.02	2.4 ± 0.8	69 ± 14	0.016 ± 0.004
0.05	7.6 ± 1.0	−3.6 ± 4.0	0.013 ± 0.006
0.08	12 ± 4	−72 ± 33	0.017 ± 0.009

increases below T_s, it saturates toward 1.2, following an order parameter of the nematic order, as seen in the inset of Fig. 9(a) where the data below T_s reported by Kitagawa *et al.* [23] are included for comparison. The value of $|\nu_a - \nu_b|/|\nu_a + \nu_b|$ over one in the orthorhombic phase indicates that the principal z axis changes to the a or b axis from the c axis [23]. In $Ba(Fe_{1-x}Co_x)_2As_2$ with $x = 0.02$, η gradually increases on cooling to T_s, obeying the CW law with the parameter values listed in Table I. It saturates to the value of 0.9 below T_s where the direction of the EFG principal axes at the As00 site remains unchanged. In the $x = 0.08$ sample with the SC phase and no orthorhombic AFM phase, η obeys the CW law as seen in Fig. 9(a). These characteristics of η in the tetragonal phase of $Ba(Fe_{1-x}Co_x)_2As_2$ are more easily seen in the contour plot of $\eta - \eta_0$ as a function of T and x on the phase diagram as seen in Fig. 1. The η monotonically increases with increasing x and shows a maximum at low temperatures around $x \sim 0.08$ in the x range of $x \leqslant 0.08$, whereas T_η changes from positive to negative signs at $x_c \sim 0.05$ with increasing x. This characteristic behavior of η is similar to the behavior of nematic susceptibility obtained by the elastic resistivity [3], electronic Raman scattering [40,41], share modulus C_{66} [43,44], and Yang's modulus $Y_{[110]}$ [51,52] measurements on $Ba(Fe_{1-x}Co_x)_2As_2$. In particular, the x dependence of T_η agrees with that of the Weiss temperature in the Raman nematic susceptibility, T_0, [40,41] (see Fig. 1) as discussed in Ref. [50]. This means that η may monitor nematic susceptibility in the absence of a coupling to the elastic strain [52], although this should be confirmed from a theoretical point of view. Thus, η is concluded to be governed by the nematic susceptibility in the tetragonal phase of $Ba(Fe_{1-x}Co_x)_2As_2$. Also the critical concentration x_c at which η diverges at $T = 0$ K is consistent with $x_c = 0.055$, where the Weiss temperature of the Raman nematic susceptibility T_0 becomes zero, and is located near the nematic quantum critical point in the SC phase x_{QCP} estimated by Raman response [53].

As seen in Fig. 9(b), $|\nu_a + \nu_b|$ gradually decreases with decreasing T in all the samples and is almost x independent. This means that the carrier is almost not doped into the As site by the Co doping, and is different from the behavior of ν_Q in $LaFeAsO_{1-\delta}$ where ν_Q is dependent on δ as $\nu_Q = 8.7, 9.5$, and $\sim$10 MHz for $\delta = 0$ with the absence of the SC transition, 0.25 with $T_c = 20$ K, and 0.4 with $T_c = 28$ K, respectively [54]. Based on these results, the ν_Q value at the As site in the iron-based superconductors is considered to be largely dependent on their local structure and the valence state of ions surrounding As. In summary, we can conclude that the nonzero value of the EFG asymmetry parameter clearly η shows the local breaking from the C_4 symmetry to the C_2 symmetry and obeys the CW law in the wide T and x region in the tetragonal phase of $Ba(Fe_{1-x}Co_x)_2As_2$.

IV. SUMMARY

We have made ^{75}As NMR measurements on single crystals to study the in-plane anisotropy of the electric field gradient at the As sites in $Ba(Fe_{1-x}Co_x)_2As_2$ with $x = 0$, 0.02, 0.05, and 0.08. We observed NMR spectra coming from the As sites with no, one, and two Co atoms at the nearest-neighbor Fe sites. From the angular dependence of the electric field gradient at the As00 site with no Co atom, we found that there is locally the symmetry breaking from C_4 to C_2 even in the tetragonal phase of all the samples and in a relatively wide temperature range. The symmetry breaking was concluded to come from the local orthorhombic domains induced by Co impurity, lattice imperfection, and so on. The asymmetry parameter of the electric field gradient η was found to obey the Curie-Weiss law and was inferred to be governed by nematic susceptibility.

ACKNOWLEDGMENTS

The authors would like to thank Y. Yamakawa, H. Kontani, and Y. Shimizu for useful information and discussion, and S. Inoue for technical support. This study was supported by KAKENHI (Grants No. JP16H04012 and No. JP15K05167) from the Japan Society for the Promotion of Science. One of the authors, M.T., was also supported by the Program for Leading Graduate Schools entitled "Integrative Graduate Education and Research Program in Green Natural Sciences."

[1] J.-H. Chu, J. G. Analytis, K. De Greve, P. L McMahon, Z. Islam, Y. Yamamoto, and I. R. Fisher, Science **329**, 824 (2010).

[2] M. Yi, D. H. Lu, J.-H. Chu, J. G. Analytis, A. P. Sorinia, A. F. Kemper, B. Moritz, S.-K. Mod, R. G. Moore, M. Hashimoto, W.-S. Lee, Z. Hussain, T. P. Devereaux, I. R. Fisher, and Z.-X. Shen, Proc. Natl. Acad. Sci. USA **108**, 6878 (2011).

[3] J.-H. Chu, H.-H. Kuo, J. G. Analytis, and I. R. Fisher, Science **337**, 710 (2012).

[4] R. M. Fernandes, A. V. Chubukov, and J. Schmalian, Nat. Phys. **10**, 97 (2014).

[5] H. Luetkens, H.-H. Klauss, M. Kraken, F. J. Litterst, T. Dellmann, R. Klingeler, C. Hess, R. Khasanov, A. Amato, C. Baines, M. Kosmala, O. J. Schumann, M. Braden, J. Hamann-Borrero, N. Leps, A. Kondrat, G. Behr, J. Werner, and B. Büchner, Nat. Mater. **8**, 305 (2009).

[6] X. F. Wang, T. Wu, G. Wu, R. H. Liu, H. Chen, Y. L. Xie, and X. H. Chen, New J. Phys. **11**, 045003 (2009).

[7] Y. Mizuguchi and Y. Takano, J. Phys. Soc. Jpn. **79**, 102001 (2010).

[8] S. Nandi, M. G. Kim, A. Kreyssig, R. M. Fernandes, D. K. Pratt, A. Thaler, N. Ni, S. L. Bud'ko, P. C. Canfield, J. Schmalian, R. J. McQueeney, and A. I. Goldman, Phys. Rev. Lett. **104**, 057006 (2010).

[9] M. G. Kim, R. M. Fernandes, A. Kreyssig, J. W. Kim, A. Thaler, S. L. Bud'ko, P. C. Canfield, R. J. McQueeney, J. Schmalian, and A. I. Goldman, Phys. Rev. B **83**, 134522 (2011).

[10] H.-H. Kuo, J.-H. Chu, J. C. Palmstrom, S. A. Kivelson, and I. R. Fisher, Science **352**, 958 (2016).

[11] S. Kasahara, H. J. Shi, K. Hashimoto, S. Tonegawa, Y. Mizukami, T. Shibauchi, K. Sugimoto, T. Fukuda, T. Terashima, A. H. Nevidomskyy, and Y. Matsuda, Nature (London) **486**, 382 (2012).

[12] K. Ikeuchi, M. Sato, S. Li, M. Toyoda, Y. Kobayashi, M. Itoh, P. Miao, S. Torii, Y. Ishikawa, and T. Kamiyama, J. Phys.: Conf. Ser. **592**, 012071 (2015).

[13] F. Kretzschmar, T. Böhm, U. Karahasanovic, B. Muschler, A. Baum, D. Jost, J. Schmalian, S. Caprara, M. Grilli, C. Di Castro, J. G. Analytis, J.-H. Chu, I. R. Fisher, and R. Hackl, Nat. Phys. **12**, 560 (2016).

[14] H. Kontani and S. Onari, Phys. Rev. Lett. **104**, 157001 (2010).

[15] Y. Inoue, Y. Yamakawa, and H. Kontani, Phys. Rev. B **85**, 224506 (2012).

[16] S. Onari and H. Kontani, Phys. Rev. B **96**, 094527 (2017).

[17] R. M. Fernandes, A. E. Böhmer, C. Meingast, and J. Schmalian, Phys. Rev. Lett. **111**, 137001 (2013).

[18] M. Breitkreiz, P. M. R. Brydon, and C. Timm, Phys. Rev. B **90**, 121104(R) (2014).

[19] H. Yamase and R. Zeyher, New J. Phys. **17**, 073030 (2015).

[20] M. Schütt, J. Schmalian, and Rafael M. Fernandes, Phys. Rev. B **94**, 075111 (2016).

[21] H. Fukazawa, K. Hirayama, K. Kondo, T. Yamazaki, Y. Kohori, N. Takeshita, K. Miyazawa, H. Kito, H. Eisaki, and A. Iyo, J. Phys. Soc. Jpn. **77**, 093706 (2008).

[22] F. Ning, K. Ahilan, T. Imai, A. S. Sefat, R. Jin, M. A. McGuire, B. C. Sales, and D. Mandrus, J. Phys. Soc. Jpn. **77**, 103705 (2008).

[23] K. Kitagawa, N. Katayama, K. Ohgushi, M. Yoshida, and M. Takigawa, J. Phys. Soc. Jpn. **77**, 114709 (2008).

[24] S.-H. Baek, T. Klimczuk, F. Ronning, E. D. Bauer, J. D. Thompson, and N. J. Curro, Phys. Rev. B **78**, 212509 (2008).

[25] F. Ning, K. Ahilan, T. Imai, A. S. Sefat, R. Jin, M. A. McGuire, B. C. Sales, and D. Mandrus, J. Phys. Soc. Jpn. **78**, 013711 (2009).

[26] F. L. Ning, K. Ahilan, T. Imai, A. S. Sefat, R. Jin, M. A. McGuire, B. C. Sales, and D. Mandrus, Phys. Rev. B **79**, 140506(R) (2009).

[27] F. L. Ning, K. Ahilan, T. Imai, A. S. Sefat, M. A. McGuire, B. C. Sales, D. Mandrus, P. Cheng, B. Shen, and H.-H. Wen, Phys. Rev. Lett. **104**, 037001 (2010).

[28] A. Smerald and N. Shannon, Phys. Rev. B **84**, 184437 (2011).

[29] D. LeBoeuf, Y. Texier, M. Boselli, A. Forget, D. Colson, and J. Bobroff, Phys. Rev. B **89**, 035114 (2014).

[30] H.-J. Grafe, U. Gräfe, A. P. Dioguardi, N. J. Curro, S. Aswartham, S. Wurmehl, and B. Büchner, Phys. Rev. B **90**, 094519 (2014).

[31] F. L. Ning, M. Fu, D. A. Torchetti, T. Imai, A. S. Sefat, P. Cheng, B. Shen, and H.-H. Wen, Phys. Rev. B **89**, 214511 (2014).

[32] P. Wiecki, B. Roy, D. C. Johnston, S. L. Bud'ko, P. C. Canfield, and Y. Furukawa, Phys. Rev. Lett. **115**, 137001 (2015).

[33] Y. Kobayashi, A. Ichikawa, M. Toyoda, M. Itoh, and M. Sato, J. Kore. Phys. Soc. **63**, 481 (2013).

[34] M. Toyoda, Y. Kobayashi, M. Itoh, and M. Sato, J. Phys.: Conf. Ser. **568**, 022029 (2014).

[35] T. Iye, M.-H. Julien, H. Mayaffre, M. Horvatić, C. Berthier, K. Ishida, H. Ikeda, S. Kasahara, T. Shibauchi, and Y. Matsuda, J. Phys. Soc. Jpn. **84**, 043705 (2015).

[36] T. Kissikov, R. Sarkar, M. Lawson, B. T. Bush, E. I. Timmons, M. A. Tanatar, R. Prozorov, S. L. Bud'ko, P. C. Canfield, R. M. Fernandes, W. F. Goh, W. E. Pickett, and N. J. Curro, Phys. Rev. B **96**, 241108(R) (2017).

[37] A. P. Dioguardi, M. M. Lawson, B. T. Bush, J. Crocker, K. R. Shirer, D. M. Nisson, T. Kissikov, S. Ran, S. L. Bud'ko, P. C. Canfield, S. Yuan, P. L. Kuhns, A. P. Reyes, H.-J. Grafe, and N. J. Curro, Phys. Rev. B **92**, 165116 (2015).

[38] T. Kissikov, A. P. Dioguardi, E. I. Timmons, M. A. Tanatar, R. Prozorov, S. L. Bud'ko, P. C. Canfield, R. M. Fernandes, and N. J. Curro, Phys. Rev. B **94**, 165123 (2016).

[39] A. P. Dioguardi, T. Kissikov, C. H. Lin, K. R. Shirer, M. M. Lawson, H.-J. Grafe, J.-H. Chu, I. R. Fisher, R. M. Fernandes, and N. J. Curro, Phys. Rev. Lett. **116**, 107202 (2016).

[40] Y. Gallais, R. M. Fernandes, I. Paul, L. Chauvière, Y.-X. Yang, M.-A. Méasson, M. Cazayous, A. Sacuto, D. Colson, and A. Forget, Phys. Rev. Lett. **111**, 267001 (2013).

[41] Y. Gallais and I. Paul, C. R. Phys. **17**, 113 (2016).

[42] N. Ni, M. E. Tillman, J.-Q. Yan, A. Kracher, S. T. Hannahs, S. L. Bud'ko, and P. C. Canfield, Phys. Rev. B **78**, 214515 (2008).

[43] T. Goto, R. Kurihara, K. Araki, K. Mitsumoto, M. Akatsu, Y. Nemoto, S. Tatematsu, and M. Sato, J. Phys. Soc. Jpn. **80**, 073702 (2011).

[44] M. Yoshizawa, D. Kimura, T. Chiba, S. Simayi, Y. Nakanishi, K. Kihou, C.-H. Lee, A. Iyo, H. Eisaki, M. Nakajima, and S. Uchida, J. Phys. Soc. Jpn. **81**, 024604 (2012).

[45] A. Abragam, *The Principles of Nuclear Magnetism* (Oxford University Press, Oxford, UK, 1961).

[46] J. L. Niedziela, M. A. McGuire, and T. Egami, Phys. Rev. B **86**, 174113 (2012).

[47] G. M. Volkoff, Can. J. Phys. **31**, 820 (1953).

[48] M. Itoh, I. Yamauchi, T. Kozuka, T. Suzuki, T. Yamauchi, J. I. Yamaura, and Y. Ueda, Phys. Rev B **74**, 054434 (2006).

[49] S. Ideta, T. Yoshida, I. Nishi, A. Fujimori, Y. Kotani, K. Ono, Y. Nakashima, S. Yamaichi, T. Sasagawa, M. Nakajima, K. Kihou, Y. Tomioka, C. H. Lee, A. Iyo, H. Eisaki, T. Ito, S. Uchida, and R. Arita, Phys. Rev. Lett. **110**, 107007 (2013).

[50] M. Toyoda, Y. Kobayashi, and M. Itoh, Phys. Rev. B **97**, 094515 (2018).

[51] A. E. Böhmer, P. Burger, F. Hardy, T. Wolf, P. Schweiss, R. Fromknecht, M. Reinecker, W. Schranz, and C. Meingast, Phys. Rev. Lett. **112**, 047001 (2014).

[52] A. E. Böhmer and C. Meingast, C. R. Phys. **17**, 90 (2016).

[53] Y. Gallais, I. Paul, L. Chauvière, and J. Schmalian, Phys. Rev. Lett. **116**, 017001 (2016).

[54] H. Mukuda, N. Terasaki, H. Kinouchi, M. Yashima, Y. Kitaoka, S. Suzuki, S. Miyasaka, S. Tajima, K. Miyazawa, P. Shirage, H. Kito, H. Eisaki, and A. Iyo, J. Phys. Soc. Jpn. **77**, 093704 (2008).